

# Enhancing Monocular Height Estimation via Weak Supervision from Imperfect Labels

Sining Chen, Yilei Shi, *Member, IEEE*, and Xiao Xiang Zhu, *Fellow, IEEE*

**Abstract**—Monocular height estimation is considered the most efficient and cost-effective means of 3D perception in remote sensing, and it has attracted much attention since the emergence of deep learning. While training neural networks requires a large amount of data, data with perfect labels are scarce and only available within developed regions. The trained models therefore lack generalizability, which limits the potential for large-scale application of existing methods. We tackle this problem for the first time, by introducing data with imperfect labels into training pixel-wise height estimation networks, including labels that are incomplete, inexact, and inaccurate compared to high-quality labels. We propose an ensemble-based pipeline compatible with any monocular height estimation network. Taking the challenges of noisy labels, domain shift, and long-tailed distribution of height values into consideration, we carefully design the architecture and loss functions to leverage the information concealed in imperfect labels using weak supervision through balanced soft losses and ordinal constraints. We conduct extensive experiments on two datasets with different resolutions, DFC23 (0.5 to 1 m) and GBH (3 m). The results indicate that the proposed pipeline outperforms baselines by achieving more balanced performance across various domains, leading to improvements of average root mean square errors up to 22.94 %, and 18.62 % on DFC23 and GBH, respectively. The efficacy of each design component is validated through ablation studies. Code is available at <https://github.com/zhu-xlab/weakim2h>.

**Index Terms**—monocular height estimation, weak supervision, noisy label, incomplete label

## I. INTRODUCTION

THREE-DIMENSIONAL perception in remote sensing is attracting much attention, as the acquired 3D information is of great significance and is crucial for many applications. In particular, modeling buildings in 3D improves our understanding of the built environment, because building heights and the building volumes that can be derived from them correlate well with urban anthropogenic factors, such as population density [1], [2], [3], energy consumption [4], [5] and solar potential [6], [7], [8], and urban heat island effects [9], [10], [11]. Moreover, monitoring forests in 3D enhances our knowledge of the global carbon reservoir [12], [13], [14], and plays an important role towards climate adaptation [15].

S. Chen and X. Zhu are with the Chair of Data Science in Earth Observation, Technical University of Munich (TUM), 80333 Munich, Germany and also with the Munich Center for Machine Learning (e-mail: [sining.chen@tum.de](mailto:sining.chen@tum.de); [xiaoxiang.zhu@tum.de](mailto:xiaoxiang.zhu@tum.de)).

Y. Shi is with the School of Engineering and Design, Technical University of Munich (TUM), 80333 Munich, Germany (e-mail: [yilei.shi@tum.de](mailto:yilei.shi@tum.de)).

The work is supported by German Federal Ministry for Economic Affairs and Climate Action in the framework of the "national center of excellence ML4Earth" (grant number: 50EE2201C) and by Munich Center for Machine Learning, by the TUM Georg Nemetschek Institute for Artificial Intelligence for the Built World as part of the AI4TWINNING project and by the Munich Center for Machine Learning.

Among all the means of 3D perception in remote sensing, methods based on single images are the most efficient and cost-effective. These advantages encourage large-scale applications of such methods in order to benefit the Global South. Technically, the 3D information is retrieved from single remote sensing images via monocular height estimation.

Since the emergence of deep learning, there has been extensive research on deep learning-based monocular height estimation. While generic fully convolutional neural networks are adopted for such purposes [16], [17], [18], various customized networks are proposed towards better performance [19], [20], [21], [22], [23], [24]. As more and more novel techniques have been proposed and rapidly popularized, they have also been adapted for monocular height estimation. Nonetheless, current research in monocular height estimation still relies on sufficient data with well-annotated labels, and does not address one major issue in real-world cases, that is, the limited data with perfect labels and plenty of data with imperfect labels. To elaborate, perfect labels for monocular height estimation are only possible with LiDAR observations, which are costly. As a result, such labels are mainly available in developed regions such as North America and Europe. Models trained on these data usually perform poorly on the unseen areas, which are the high-demand developing regions (*e.g.*, South America and Asia), where only imperfect labels acquired by other means are available. Only by incorporating imperfect labels can models work reasonably well in those areas.

There have been attempts to train networks with imperfect data through weakly supervised learning [25], [26], [27], [28]. However, the solutions are tailored to one specific task and problem setting, and thus cannot be adopted directly. To design a framework specifically for monocular height estimation, several aspects should be taken into account. First, there are different levels of label qualities in monocular height estimation—each requiring a distinct treatment because of different label properties. Second, given the availability of high-quality labels corresponding to the development status, the domains vary with different label qualities. Third, as one of the thorny issues, the long-tailed distribution of height values also exists in these imperfect labels [29].

To address these issues, we propose an ensemble-based framework that deals with all types of label quality. We design the training loss functions with careful consideration of the challenges. In summary, our contributions are as follows.

- To the best of our knowledge, we tackle the problem of introducing imperfect labels in training monocular height estimation networks for the first time.

- We propose an ensemble-based pipeline, compatible with all kinds of label qualities.
- We propose loss functions tailored to best exploit the supervisory information from the imperfect labels. This includes the balanced soft height loss and the ordinal constraints. We also propose the ground truth augmentation module to mitigate the blurring effect in the outputs.
- We conduct experiments on two datasets, and we demonstrate the efficacy of our proposed pipeline in learning from the imperfect labels and balancing the performance across various domains.

The remainder of the article is organized as follows. Section II gives an overview of the related works. The proposed method is described in detail in Section III, followed by Section IV describing the experiments and Section V showing the experimental results. Discussions and ablation studies are presented in Section VI. Conclusions are drawn, and further research directions are described in Section VII.

## II. RELATED WORKS

### A. Monocular Height Estimation

Monocular height estimation is the process of predicting height values from single optical images. Early works explicitly exploit shadows as cues to infer the heights of ground objects [30]. However, they are restricted to cases when shadows are clearly seen in the images, and therefore do not perform well in dense urban areas. As deep learning has achieved state-of-the-art performance in many tasks, deep learning-based monocular height estimation methods stand out due to their flexibility and capability.

Monocular height estimation, in the context of this work, refers to pixel-wise height estimation methods, which estimate a height value for each pixel. It requires neural networks for dense predictions. For this purpose, fully convolutional neural networks (FCNs) could be utilized.

On the one hand, many universal FCNs [16], [17], [18] can be adopted by removing the final activation layer to produce continuous-valued outputs. These FCNs mainly follow an encoder-decoder design, enabling the output to have the same size as that of the input. For example, U-Net [16], originally proposed for biomedical image segmentation, is one of the most popular FCNs, where several skip connections efficiently fuse features from the encoders and decoders.

On the other hand, some neural networks are specifically designed for monocular height estimation [19], [20], [21], [22], [23], [24]. For example, Mou and Zhu [19] proposed one of the pioneering neural networks for monocular height estimation. It is a lightweight encoder-decoder network with one skip connection to enable low-level feature fusion in the prediction. Amirkolaee *et al.* [20] designed a network based on U-Net with upsampling blocks and multi-level feature fusion. Xing *et al.* [21] proposed the PLNet with the gated feature aggregation module (GFAM) and the progressive refine model (PRM). Chen *et al.* [22] proposed HTC-DC Net, following the novel classification-regression paradigm, inspired by [31]. The network is enhanced via a head-tail cut (HTC) and distribution-based constraints (DC). Additionally, there have

been many attempts to introduce auxiliary tasks, in addition to height predictions, through multi-task learning [23], and to exploit generative methods such as generative adversarial networks (GAN) [24].

Although there have been extensive studies on monocular height estimation, existing studies address only cases when adequate perfect labels are available for training networks, and they do not evaluate the model's generalization performance across the various domains. In practice, these issues largely affect the utilizability of models and thus deserve more attention.

### B. Weakly Supervised Learning

Weakly supervised learning is aimed at training models efficiently with weak supervision from imperfect data, so that the intensive labor and high cost of obtaining large-scale, high-quality datasets can be reduced. It covers a broad range and varies for different tasks and problem settings. In general, it focuses on learning with incomplete, inexact, and inaccurate supervision [25]. In classification tasks, for example, semi-supervised learning makes use of unlabeled data as incomplete supervision [32], [33], [34], [35], [36]. This is addressed by multi-instance learning, which deals with inexact labels. The labels are available for bags of multiple instances, representing the class of one of them. Multi-instance learning algorithms tend to adapt single-instance supervised learning methods to the multi-instance representation [37] or *vice versa*, by transformation [38]. Another example is learning from noisy labels through inaccurate supervision via data-editing approaches [39], [40].

For regression tasks, we face a different and less-tackled problem setting, as the output space is no longer discretized into classes. One example of weakly supervised regression is monocular depth estimation in the computer vision community, a task closely related to monocular height estimation. Instead of training a network with exact depth annotations, some works attempted to use weak labels representing the depth information. For example, Chen *et al.* [26] trained monocular depth estimation networks with relative depth annotations only, *i.e.*, a pixel is closer, farther than, or equal to another pixel. The learning is done via an ordinal relation loss function. Lienen *et al.* [27] extended the pixel pairs to lists of pixels, and trained the network using a Plackett-Luce model that ranks the pixels. Inspired by these works, Xiong and Zhu [28] utilized a network pre-trained on a synthetic dataset to generate weak pseudo-labels for real-world datasets and fine-tuned the network on these to achieve label-efficient knowledge transfer in monocular height estimation.

Although works on weakly supervised learning in monocular depth estimation and monocular height estimation exist, they do not address the real-world label quality issues or model generalizability. Thus, they cannot be directly adapted to this work because the tasks and problem settings differ. There is still a need to develop novel pipelines.

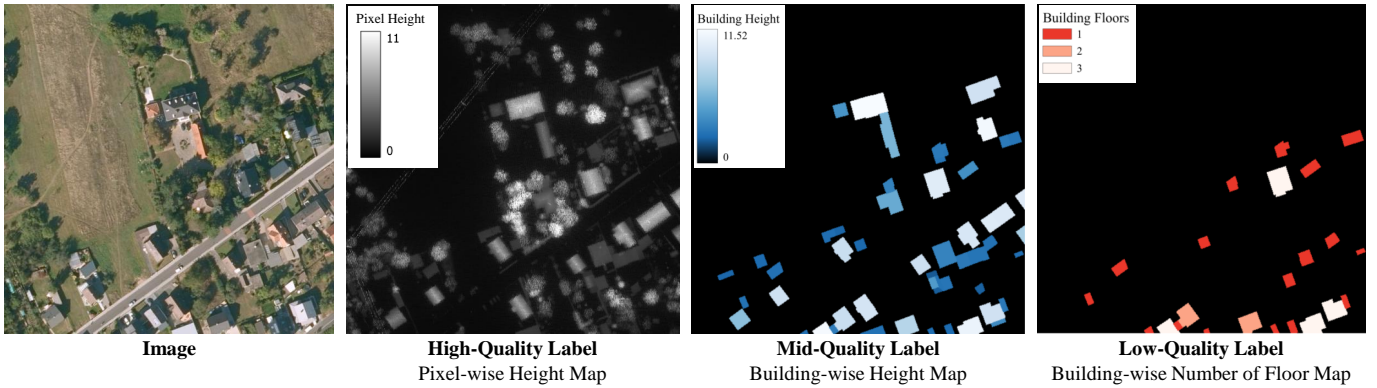


Fig. 1. Common Label Qualities for Monocular Height Estimation. Data from [41].

### III. METHODOLOGY

#### A. Problem Formation

The goal is to train a neural network for pixel-wise height estimation with labels of varying qualities (see Fig. 1). In general, these labels are categorized into high-, mid-, and low-quality.

1) *High-quality Labels*: High-quality labels are those that match the quality of the expected network outputs. More specifically, for pixel-wise height estimation networks, the labels should be pixel-wise height maps, typically delivered as normalized digital surface models (nDSMs), which fully preserve the detailed height structures when the ground sampling distance is sufficient.

These labels are ideally acquired from LiDAR observations, which account for their high cost and scarce availability.

2) *Mid-quality Labels*: Mid-quality labels are the labels with incomplete height annotations. Labels of this quality level are usually instance (building)-wise height maps generated from 3D building models. The quality can still differ depending on the level of detail (LoD) of the building models. In the worst and most common case, LoD-1 building models represent buildings as blocks, assigning one height value per building block. Therefore, although the height annotations tend to be almost correct, the finer structures on the buildings are smoothed out. When using such labels as pixel-wise ground truth, the height values may not reflect the exact height of the pixels.

These labels have higher availability because the 3D building models can be derived from cadastral profiles or other cost-effective observation methods.

3) *Low-quality Labels*: Low-quality labels refer to the labels with incomplete height annotations as well as noise. They are usually building-wise floor number maps. They are similar to mid-quality labels, except that the height values are replaced by the number of floors. On the one hand, the building-wise nature means inexactness and incompleteness. On the other hand, although strong correlations exist between building heights and building floor numbers, the relationship varies for different floor heights and thus the height information in these labels is, to some extent, noisy [42].

These labels are widely available because they can be acquired from census or volunteered geographic information (VGI) systems, for instance, OpenStreetMap (OSM) [43].

In summary, given data samples with labels of varying qualities, the goal is to include all the labels to train a pixel-wise monocular height estimation neural network.

#### B. Network Architecture

As illustrated in Fig. 2, the proposed method is an ensemble-based pipeline, where each branch accounts for a level of label quality. Based on the observation that the encoder is less sensitive to label noise [44], and in order to reduce the computational burden, the branches share the same encoder and use different decoders.

Because the labels of different levels are distributed according to geographic locations, *i.e.*, high-quality labels are more available in the developed areas, such as North America, Europe, and Oceania, while lower-quality labels are mostly seen in the less-developed areas, such as Asia and South America, the label quality might reflect the "domain" information behind it. To better use this information, a so-called "domain" classifier—more precisely, a label quality classifier—is built on top of the shared encoder. The "domain" classifier is designed as an image classification module.

The encoder and decoder can be from any height estimation network. The classifier is made up of several convolutional layers, pooling layers, followed by fully connected layers that result in "domain" class logits, and then class probabilities  $\hat{p}_c$ .

The class probabilities are used to blend the height predictions from all the branches during inference, *i.e.*, the predicted height maps  $h$  are the sum of the height maps from all the branches weighted by the class probabilities. That is,

$$\hat{h} = \sum_{c=0}^{C-1} \hat{p}_c \hat{h}^c, \quad (1)$$

where  $\hat{p}_c \in \mathbb{R}^C$ ,  $\sum_{c=0}^{C-1} \hat{p}_c = 1$  is the class probability for "domain" (quality label)  $c$  from the total  $C$  classes, and  $h^c$  is the predicted height map from the branch  $c$ .

During training, the predicted height map from the ground truth branch only is used to compute the height-related loss terms.

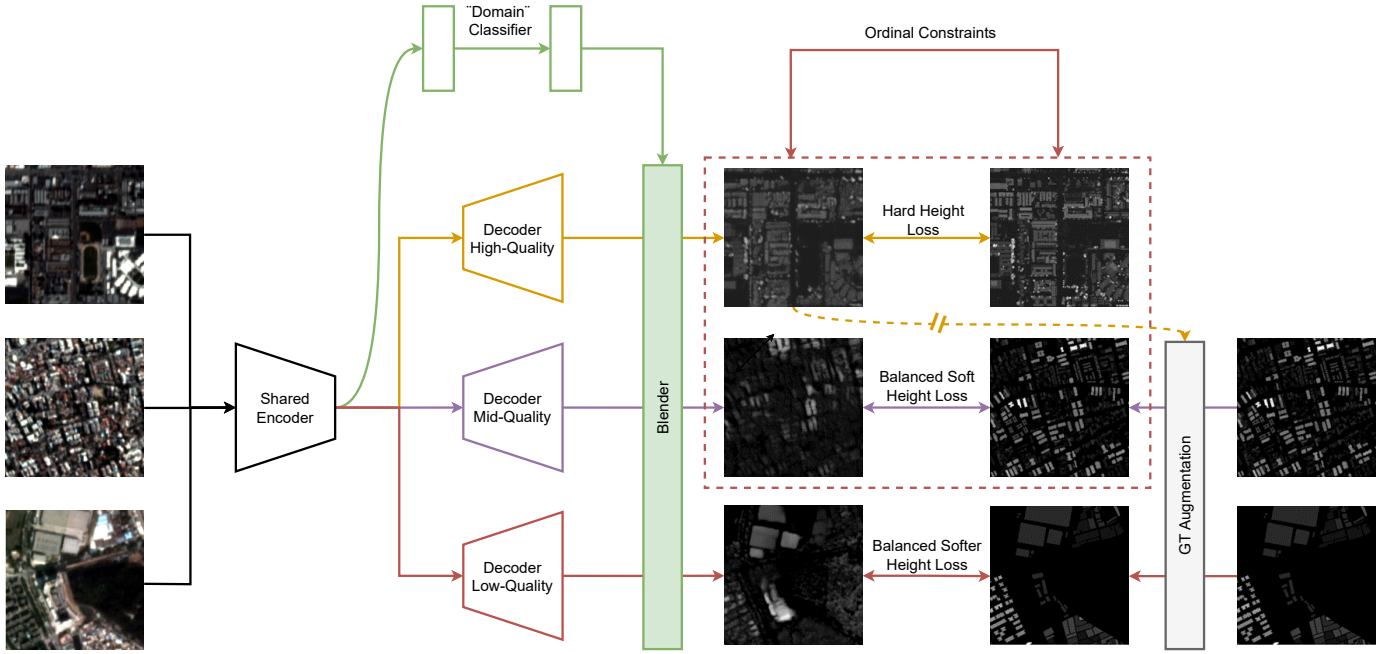


Fig. 2. Network Architecture. The network is designed as an ensemble-based network, with branches dedicated to high-quality, mid-quality, and low-quality labels, respectively. A "domain" classifier is used to classify different label qualities and blend the outputs from each branch for the final output. The outputs from the high-quality branch are also used for ground truth augmentation for the mid- and low- quality labels, where the backward gradients are stopped.

### C. Loss Functions

The optimal exploitation of imperfect labels is ensured through specifically designed loss functions, which are detailed in this section.

1) *"Domain" Classification Loss*: The "domain" classifier is supervised using the "domain" classification loss, a cross-entropy loss. It is written as

$$L_{DC} = - \sum_{c=0}^C y_c \log(\hat{p}_c), \quad (2)$$

where  $y_c$  denotes the ground truth domain labels.

2) *Hard Height Loss*: For the high-quality labels, the height annotations are assumed to be perfectly precise. Therefore, a hard height loss is applied to make the best use of the precious information. The hard height loss is defined as the standard L1 loss, written as

$$L_{HH} = \frac{1}{|\mathcal{I}|} \sum_{i \in \mathcal{I}} |\hat{h}_i - h_i|, \quad (3)$$

where  $\mathcal{I}$  is the set of image pixels,  $\hat{h}_i$  and  $h_i$  are the predicted and ground truth height values for pixel  $i$ , respectively.

3) *Balanced Soft Height Loss*: For the mid- and low-quality labels, the height annotations represent, to some extent, the accurate height information, therefore, the supervision signal should be exploited with care. The loss function should penalize the network for a sampled pixel subset only if the error is large enough to tell that the prediction deviates from the ground truth. Following this principle, we propose the balanced soft height loss.

First, a buffer around the ground truth is designed to soften the penalization from the loss function. The loss function for

a pixel applies only if the error exceeds a certain threshold, written as

$$L_{SH} = \begin{cases} 0 & |h_i - \hat{h}_i| \leq \tau \\ |h_i - \hat{h}_i| & |h_i - \hat{h}_i| > \tau \end{cases}, \quad (4)$$

where  $\tau$  is a threshold specifying the width of the buffer. In practice, the threshold is defined relative to the ground truth height values, that is

$$\tau_i = \lambda_\tau h_i \quad (5)$$

where  $\lambda_\tau$  is a hyperparameter defining the relative threshold.

Second, to further soften the loss, the loss is only applied to a sampled subset  $\mathcal{S}$ . So the balanced soft height loss is written as

$$L_{BSH} = \frac{1}{|\mathcal{S}|} \sum_{i \in \mathcal{S}} L_{SH}, \quad (6)$$

where the subset  $\mathcal{S}$  is a sampled subset with a specified number of pixels. The sampling process should be balanced to combat the effect of imbalanced height values [29]. To achieve this, all the pixels are sorted by their ground truth height values, and a sampling interval is computed by dividing the total pixel number by the sample number. The subset is then sampled based on the sampling interval.

4) *Ordinal Constraints*: Although the height information from the imperfect labels contains noise, the relative relations between pixels tend to be more trustworthy, which is, to be specific, one pixel is higher or lower than another pixel. To make full use of this relative information, an ordinal relation loss is applied as constraints.

Previously, ordinal relations were adopted for depth perception [26], [27] in the wild and efficient knowledge transfer in

monocular height estimation [28], and proven to be efficient. However, the strategy cannot be adopted as it was. It should be carefully designed with the special challenges of monocular height estimation in mind.

First, to improve the robustness of the ordinal relation ground truth, we discretize the height values into classes based on a space increasing discretization (SID) strategy [45]. That is, the continuous height range is divided into classes by intervals whose widths increase with height. Given the minimal and maximal height values,  $h_{min}$  and  $h_{max}$ , the discretization threshold  $t_k$  as the edge for class  $k$  is defined as

$$t_k = \exp(\log(h_{min}) + \frac{\log(h_{max}/h_{min})}{K}k), \quad (7)$$

where  $K$  is the total number of classes. By discretizing the height range, ground truth height values that are close are treated as equal in ordinal terms so that the inaccuracy of the ground truth information misleads the network less.

Second, different from the ordinal constraints used in [26], [28] for monocular depth estimation, only "closer" and "farther" relations, corresponding to "lower" and "higher", are enforced as constraints. The equal relation is discarded due to the inaccuracy of ground truth. The ordinal relations are written as

$$L_{OC}(\hat{h}_1, \hat{h}_2) = \begin{cases} \log(1 + \exp(\hat{h}_2 - \hat{h}_1)), & c_1 > c_2 \\ 0, & c_1 = c_2 \\ \log(1 + \exp(\hat{h}_1 - \hat{h}_2)), & c_1 < c_2 \end{cases} \quad (8)$$

where  $\hat{h}_1$  and  $\hat{h}_2$  are predicted height values for pixel 1 and pixel 2, and  $c_1$  and  $c_2$  are the ground truth height classes, respectively.

Third, bearing the long-tailed distribution in monocular height estimation [29] in mind, if the pixel pairs are sampled randomly, the learned constraints might be skewed towards the low pixels. To cope with this problem, we use a balanced random sampling strategy. Consider a case with pixels of  $M$  height classes, in total, there are

$$N_{pairs} = \binom{M}{2} = \frac{M(M-1)}{2} \quad (9)$$

types of pixel pairs. Ideally, when sampling  $S$  pixel pairs, for each type, there should be

$$N_c = \frac{S}{N_{pairs}} = \frac{2S}{M(M-1)} \quad (10)$$

pixel pairs. But the number of pixel pairs for each type is bounded by the smallest possible pair counts for all types. That is,

$$N_{min} = n_{c_1}n_{c_2}, \quad (11)$$

where  $c_1$  and  $c_2$  are the classes with the minimum and the second minimum counts over all classes. Then, for each type,

$$\hat{N} = \min(N_c, N_{min}), \quad (12)$$

pairs of pixels should be sampled. This sampling strategy ensures a balance between head and tail pixels in ordinal constraint learning.

In addition, height estimation predicts the physical nature of an object, therefore, the predicted values should be consistent regardless of the context is. This is distinct from those in monocular depth estimation. Inspired by this, cross-image relations are applied to enforce the network to learn consistent ordinal relations. In practice, predicted height maps are flattened and concatenated into a single vector to compute the ordinal constraint.

5) *Total Training Loss*: The pipeline is trained via the total training loss  $\mathcal{L}$ , which is the sum of the abovementioned loss terms, namely, the "domain" classification loss, the hard height loss, the balanced soft height loss, and the ordinal constraints. That is

$$\mathcal{L} = L_{DC} + L_{HH} + L_{BSH} + L_{OC} \quad (13)$$

#### D. Ground Truth Augmentation

As observed in experiments, which are described in Section VI-B4, the incomplete labels lead to over-blurred predictions from the mid- and low-quality branches. To mitigate this effect, we propose a ground truth augmentation module to generate pseudo-high-quality labels to refine the outputs.

To simulate real-world height maps, fine details must be injected while preserving the accuracy of the original ground truth labels. It turns out that the predictions from the high-quality label branch serve as appropriate candidates to augment the ground truth. They are weighted and added to the original ground truth to supervise the mid- and low-quality branches. To reduce the side effect of false supervisory signal introduced by the false predictions, first, a threshold is used to filter the trustworthy predictions from the high-quality branch. Second, dropout is used to enable both original and augmented ground truth seen during training. The overall process is defined as

$$h_{aug} = \mathcal{M} \odot \mathcal{H} + (1 - \mathcal{M})h, \quad (14)$$

where

$$\mathcal{H} = \eta h + (1 - \eta)\hat{h}^0, \quad (15)$$

$$\mathcal{M}_i = \begin{cases} 1, & |h_i - \hat{h}_i^0| < \omega \text{ and not dropout} \\ 0, & \text{else} \end{cases} \quad (16)$$

$h_{aug}$  is the augmented ground truth height map, serving as pseudo-high-quality labels.  $h$  is the original ground truth height map,  $\hat{h}^0$  is the predicted height map from the high-quality branch.  $\eta$  and  $\omega$  are hyperparameters, defining the weights of the two height maps and the threshold of prediction errors, respectively. The weight  $\eta$  decays during training, for epoch  $t$ , it is written as

$$\eta_{t+1} = \max(\eta_t \alpha, 0.5) \quad (17)$$

where  $\alpha$  is a hyperparameter representing the decay effect. Similar to the threshold defined in the soft height loss, the threshold  $\omega$  is defined relative to the ground truth values, similar to the soft height loss.

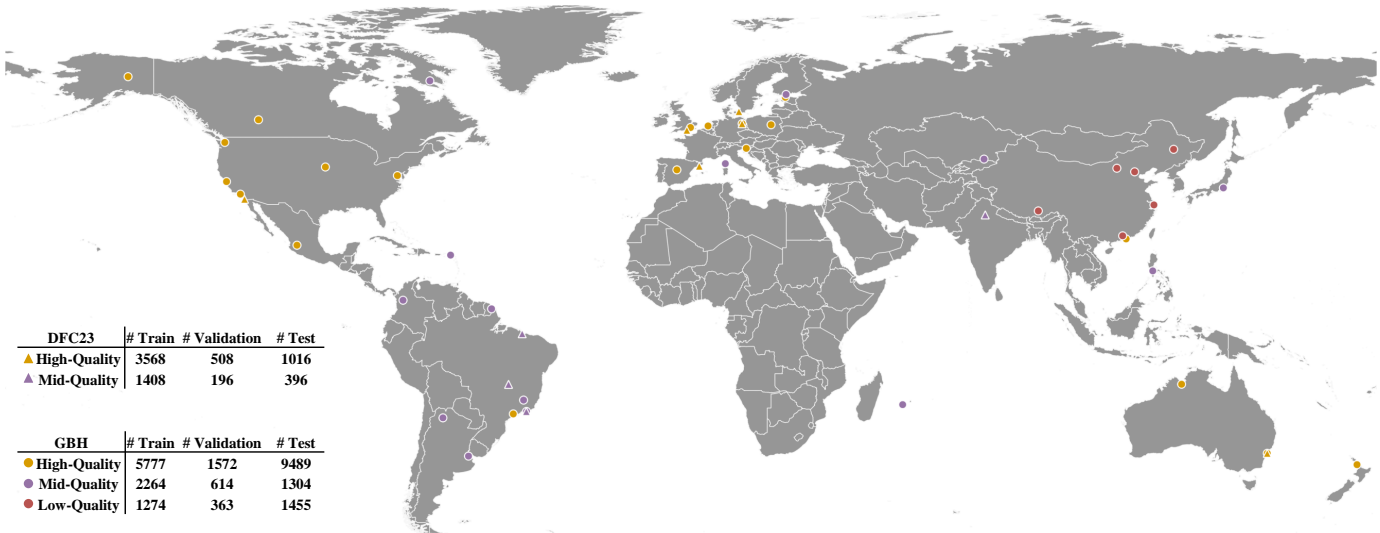


Fig. 3. Distribution of Data Samples.

## IV. EXPERIMENTS

### A. Datasets

To validate our proposed pipeline, we need datasets that fulfill specific criteria. First, the dataset should cover a large variety of geolocations, *i.e.*, the domains. Second, the dataset should contain or could be adapted to have mid- and low-quality labels. Based on these criteria, two datasets are short-listed.

1) *DFC23*: DFC23 (Data Fusion Contest 23) dataset [46], [47] is tailored for large-scale fine-grained building classification for semantic urban reconstruction. It contains images acquired by the SuperView-1 (“GaoJing” in Chinese), Gaofen-2, and Gaofen-3 satellites, normalized digital surface models (nDSMs) produced from stereo images from Gaofen-7 and World-View 1 and 2. The images and nDSMs have spatial resolutions of 0.5 to 1 m, and 2 m, respectively. The dataset is globally distributed, covering 17 cities on 6 continents.

The dataset comprises 1,773 patches with size  $512 \times 512$ , which are split into training, validation, and test sets in a 74:16:20 ratio. The patches are cropped into 7,092 smaller patches of  $256 \times 256$ . The data distribution is illustrated in Fig. 3. The dataset is adapted as follows to better align with the scope of the work:

- The dataset is split according to the continents: 5,092 patches in North America, Europe, and Oceania are considered to have high-quality labels, and the other 2,000 patches from other continents are considered to have mid-quality labels.
- The mid-quality labels are processed to have uniform height values within each building instance, and the non-building pixels are set to zero.
- A test set is constructed with samples from all cities to observe the model’s performance in different domains. Specifically, the high-quality test set is seen as the in-domain test set, and other test sets, namely, Brasilia, New

Delhi, Sao Luis, and Rio de Janeiro, are used as out-of-domain test sets.

2) *GBH*: GBH (Global Building Height) dataset is a customized dataset. The dataset was designed to combine both diversity and volume of data samples in monocular height estimation. The resulting dataset is made up of optical remote sensing images acquired by PLANET satellites, height maps generated from open LiDAR observations or building models, and building footprint maps.

The dataset of the version used in this work covers 40 cities around the globe, dating from 2013 to 2021. The ground sampling distance is 3 m for the 24,112 patches of size  $256 \times 256$ , among which 16,838 patches are high-quality labeled, and 4,182 patches are mid-quality labeled. The dataset also includes 3,092 samples labeled with low-quality information in the form of building floor counts. An overview of the dataset can be seen in Fig. 3. The dataset is used as follows:

- The dataset is split into high-, mid-, and low-quality sets. For each set, training, validation, and test subsets are created.
- The original data samples are labeled with different qualities, so no label processing is needed.
- Besides the two test sets mentioned above, four cities are left-out, reserved exclusively for testing purposes, *i.e.*, they are never seen during training. They are Los Angeles (USA), Sao Paulo (Brazil), Medellin (Colombia), and Guangzhou (China).
- The test sets are categorized as in-domain or out-of-domain according to their geographic locations and qualities of available labels. Specifically, the high-quality test set and Los Angeles form the in-domain test sets, and mid-/low-quality test set, Sao Paulo, Medellin, and Guangzhou constitute the out-of-domain test sets.

## B. Evaluation Metrics

The models are evaluated using the building-wise root mean square error (RMSE). This is computed under the assumption of LoD-1 building models for each building instance, *i.e.*, only the median height value within each building instance is considered. For each experiment, the average building-wise RMSEs are computed for the in-domain, out-of-domain, and combined test sets to assess the model's generalization capability across diverse domains.

## C. Implementation Details

The pipeline is validated using three backbone networks: U-Net [16], IM2HEIGHT [19], and AdaBins [31]. U-Net is a universal fully convolutional network for dense prediction and yields competitive results in monocular height estimation. IM2HEIGHT is one of the pioneering specially designed monocular height estimation networks. AdaBins, originally proposed for monocular depth estimation, serves as the base for HTC-DC Net [22], a monocular height estimation network that achieves the state-of-the-art performance. To adapt the U-Net for monocular height estimation, the final activation layer is removed.

For each baseline network, the following experiments are conducted for comparison.

- The baseline network is trained only on data with high-quality labels.
- The baseline network is trained only on data with mid- or mid-/low-quality labels as pixel-wise supervision.
- The baseline network is trained on all the data, where the mid- or mid-/low-quality labels are treated as pixel-wise supervision.
- The proposed pipeline, backboneed by the baseline network, is trained on all the data.

For the DFC23 dataset, the ensemble consists of two branches: one for high-quality and one for mid-quality labels, while for the GBH dataset, an additional low-quality branch is equipped. For the soft height loss, the error threshold is set as 0.3 of the ground truth height for mid-quality labels, and 0.5 of the ground truth height for low-quality labels. The soft height loss is computed on a sampled set of 10 % pixels for both mid- and low-quality labels. For the ordinal constraints, the height values are discretized into 20 classes. The constraint is applied to  $H \times W$  pairs of pixels, where  $H$  and  $W$  are the height and width of each image. For the ground truth augmentation, the error threshold is set as 0.1 of the ground truth height value to filter the trustworthy predictions from the high-quality branch, and the dropout probability is set as 0.3. The weighting parameter  $\eta$  is initialized to 1, and decays with the factor 0.99 at each epoch.

The networks are trained for 200 epochs with the Adam optimizer, and a learning rate of  $1e-4$ . The model from the epoch with the best validation performance is selected for testing. Each experiment is repeated three times, and the average performance metrics are reported.

## V. RESULTS

The quantitative results are shown in Table I and Table II. The qualitative results are presented in Fig. 4 and Fig. 5.

Overall, the proposed pipeline improves model performance in regions with imperfect labels, while maintaining comparable results in areas with high-quality labels.

### A. DFC23

As seen in Table I, our proposed pipelines consistently enhance the performance of the backbone networks, achieving the lowest average building-wise RMSE across all configurations. Specifically, the improvements over the best-performing baseline (H+M) are 7.90 %, 14.40 %, and 22.94 %, for U-Net, IM2HEIGHT, and AdaBins B5, respectively. Furthermore, the pipelines deliver more balanced performance across various domains: in cities with high-quality labels, performance remains comparable to the baseline, while in cities with only mid-quality labels, the improvements are significantly more substantial.

These quantitative gains are also reflected in the qualitative results shown in Fig. 4. The qualitative results in Fig. 4 show that our pipelines generate height maps with better-preserved building structures. While the differences are subtle in areas with high-quality labels, they are more pronounced in cities with only mid-quality labels, where our method yields sharper edges and more clearly defined buildings.

### B. GBH

The GBH dataset encompasses a broader range of cities, including those with low-quality labels, enabling evaluation of improvements in such regions. As reported in Table II, our proposed pipelines significantly outperform the baseline networks (H+M/L) in terms of average building-wise RMSE, with improvements of 13.61 %, 18.62 %, and 14.47 %, for U-Net, IM2HEIGHT, and AdaBins B5, respectively. These gains are most significant in cities with only mid- or low-quality labels, where our approach consistently achieves the lowest out-of-domain average RMSEs. The improvements in these challenging domains largely offset the minor performance reductions observed on the high-quality test set and in Los Angeles.

The qualitative results in Fig. 5 further demonstrate the preservation of fine-grained structural details by our proposed pipelines, supporting the quantitative findings. These visualizations also suggest that our pipelines effectively combine the strengths of networks trained on different subsets of the training data.

In summary, the proposed pipelines enhance the baseline networks by leveraging imperfect labels to achieve significantly better performance in cities with lower-quality annotations, while maintaining comparable results elsewhere. This results in a more balanced overall performance across diverse domains. These results highlight the robustness and adaptability of our method across diverse urban environments and varying label qualities.

## VI. DISCUSSION

### A. Model Generalizability with Different Training Data

We have conducted experiments using different training datasets on three monocular height estimation networks and

TABLE I

EXPERIMENTAL RESULTS ON DFC23. BUILDING-WISE RMSES ARE REPORTED IN METERS. EACH EXPERIMENT IS CONDUCTED THREE TIMES, AND THE AVERAGE METRICS ARE PRESENTED. H: HIGH-QUALITY; M: MID-QUALITY. THE BEST RESULT IN EACH SET IS HIGHLIGHTED IN GREEN, AND THE SECOND-BEST IN BLUE.

Network	Trained on	In-Domain			Out-of-Domain			Average	Average
		High-Quality Test Set	Brasilia	New Delhi	Sao Luis	Rio de Janeiro			
U-Net [16]	H	<b>4.3308</b>	6.2238	11.1197	6.8789	13.4260	9.4121	8.3958	
	M	15.0725	<b>1.8674</b>	<b>4.3610</b>	<b>2.0855</b>	<b>7.2211</b>	<b>3.8837</b>	6.1215	
	H+M	5.3343	2.8716	4.8708	2.6416	8.9380	4.8305	<b>4.9312</b>	
ours + U-Net	H+M	<b>4.8461</b>	<b>2.4613</b>	<b>4.7726</b>	<b>2.6402</b>	<b>7.9878</b>	<b>4.4655</b>	<b>4.5416</b>	
IM2HEIGHT [19]	H	<b>5.8326</b>	5.1242	10.6451	7.3185	13.9272	9.2538	8.5695	
	M	14.8098	2.4793	5.6552	2.5868	<b>8.0383</b>	<b>4.6899</b>	6.7139	
	H+M	<b>5.9918</b>	<b>2.4590</b>	<b>5.6141</b>	<b>2.5631</b>	8.4025	4.7597	<b>5.0061</b>	
ours + IM2HEIGHT	H+M	6.0651	<b>1.8587</b>	<b>3.9865</b>	<b>2.1776</b>	<b>7.3389</b>	<b>3.8404</b>	<b>4.2853</b>	
AdaBins B5 [31]	H	<b>4.2442</b>	6.5472	9.9179	7.1489	12.4282	9.0105	8.0573	
	M	13.2865	<b>2.2143</b>	<b>4.8853</b>	2.5159	<b>7.5285</b>	<b>4.2860</b>	6.0861	
	H+M	5.9559	2.6537	5.6449	<b>2.4535</b>	10.3187	5.2677	<b>5.4053</b>	
ours + AdaBins B5	H+M	<b>5.6022</b>	<b>1.7491</b>	<b>3.9914</b>	<b>2.1789</b>	<b>7.3040</b>	<b>3.8059</b>	<b>4.1652</b>	

TABLE II

EXPERIMENTAL RESULTS ON GBH. BUILDING-WISE RMSES ARE REPORTED IN METERS. EACH EXPERIMENT IS CONDUCTED THREE TIMES, AND THE AVERAGE METRICS ARE PRESENTED. H: HIGH-QUALITY; M: MID-QUALITY; L: LOW-QUALITY. THE BEST RESULT IN EACH SET IS HIGHLIGHTED IN GREEN, AND THE SECOND-BEST IN BLUE.

Network	Trained on	In-Domain			Mid-/Low-Quality Test Set	Out-of-Domain			Average	Average
		High-Quality Test Set	Los Angeles	Average		Sao Paulo	Medellin	Guangzhou		
U-Net [16]	H	<b>3.8915</b>	<b>2.4214</b>	<b>3.1564</b>	16.0513	<b>6.3528</b>	<b>4.3093</b>	<b>13.7006</b>	10.1035	7.7878
	M/L	7.6104	7.8630	7.7367	<b>11.6371</b>	6.4807	4.6644	15.7384	9.6301	8.9990
	H+M/L	<b>4.0981</b>	3.6468	<b>3.8724</b>	11.7305	6.3704	4.7381	14.5750	<b>9.3535</b>	<b>7.5265</b>
ours + U-Net	H+M/L	4.2323	<b>3.5862</b>	3.9093	<b>9.2725</b>	<b>5.5070</b>	<b>3.8394</b>	<b>12.5761</b>	<b>7.7987</b>	<b>6.5023</b>
IM2HEIGHT [19]	H	<b>5.1190</b>	<b>2.9118</b>	<b>4.0154</b>	17.6651	<b>6.8923</b>	<b>4.4851</b>	<b>16.8945</b>	11.4843	<b>8.9946</b>
	M/L	8.1578	4.5641	6.3610	15.9578	7.7574	5.3270	17.9398	11.7455	9.9506
	H+M/L	<b>5.1893</b>	3.2747	<b>4.2320</b>	<b>14.8351</b>	7.4922	5.2060	17.3906	<b>11.2310</b>	8.8980
ours + IM2HEIGHT	H+M/L	5.6562	<b>3.0636</b>	4.3599	<b>10.5633</b>	<b>6.0087</b>	<b>3.9307</b>	<b>14.2240</b>	<b>8.6817</b>	<b>7.2411</b>
AdaBins B5 [31]	H	<b>4.0148</b>	<b>2.2375</b>	<b>3.1261</b>	16.2250	<b>6.4674</b>	<b>4.3789</b>	<b>13.8260</b>	10.2243	7.8583
	M/L	6.9874	4.6826	5.8350	11.8719	6.5632	4.6940	15.4551	9.6460	8.3757
	H+M/L	<b>3.9835</b>	2.6641	<b>3.3238</b>	<b>11.7416</b>	6.5350	4.7810	14.3911	<b>9.3622</b>	<b>7.3494</b>
ours + AdaBins B5	H+M/L	4.5589	<b>2.5139</b>	3.5364	<b>9.2164</b>	<b>5.2202</b>	<b>3.9779</b>	<b>12.2288</b>	<b>7.6608</b>	<b>6.2860</b>

observed that their performance varied depending on the quality and diversity of training data. This section discusses how training data quality and composition affect model generalizability.

Generally, the more diverse the data a model is exposed to during training, the better the overall performance. When trained solely on data with high-quality labels, a model tends to perform well on the corresponding test set. However, it may produce unreliable results on other test sets. For instance, as shown in Fig. 4 and Fig. 5, when evaluated on test sets outside of the high-quality domain, the predictions often become noisy, with spurious patterns from non-building objects dominating the outputs. A similar trend is observed in models trained exclusively on data with mid- and/or low-quality labels. This is reflected quantitatively, where models trained with high-quality labels achieve the lowest in-domain building-wise RMSE. However, this advantage does not extend to out-of-domain settings. The likely reason is that the noise

present in the labels prevents the model from learning correct reasoning of heights from images.

Training with data that include all label qualities is expected to yield the best generalization. However, the inclusion of imperfect labels can still harm performance by introducing noise into the learning process. This can lead to reduced accuracy in cities with high-quality annotations and even failure cases in regions with lower-quality annotations. From this perspective, our proposed pipeline extracts useful supervisory signals from noisy data through a sophisticated architecture and loss design, achieving a balanced performance over all domains.

Although our proposed pipeline demonstrates effectiveness in addressing these challenges, it is important to emphasize that data availability, particularly the quality and diversity of labels, remains the most critical factor in developing models with strong generalization capabilities.

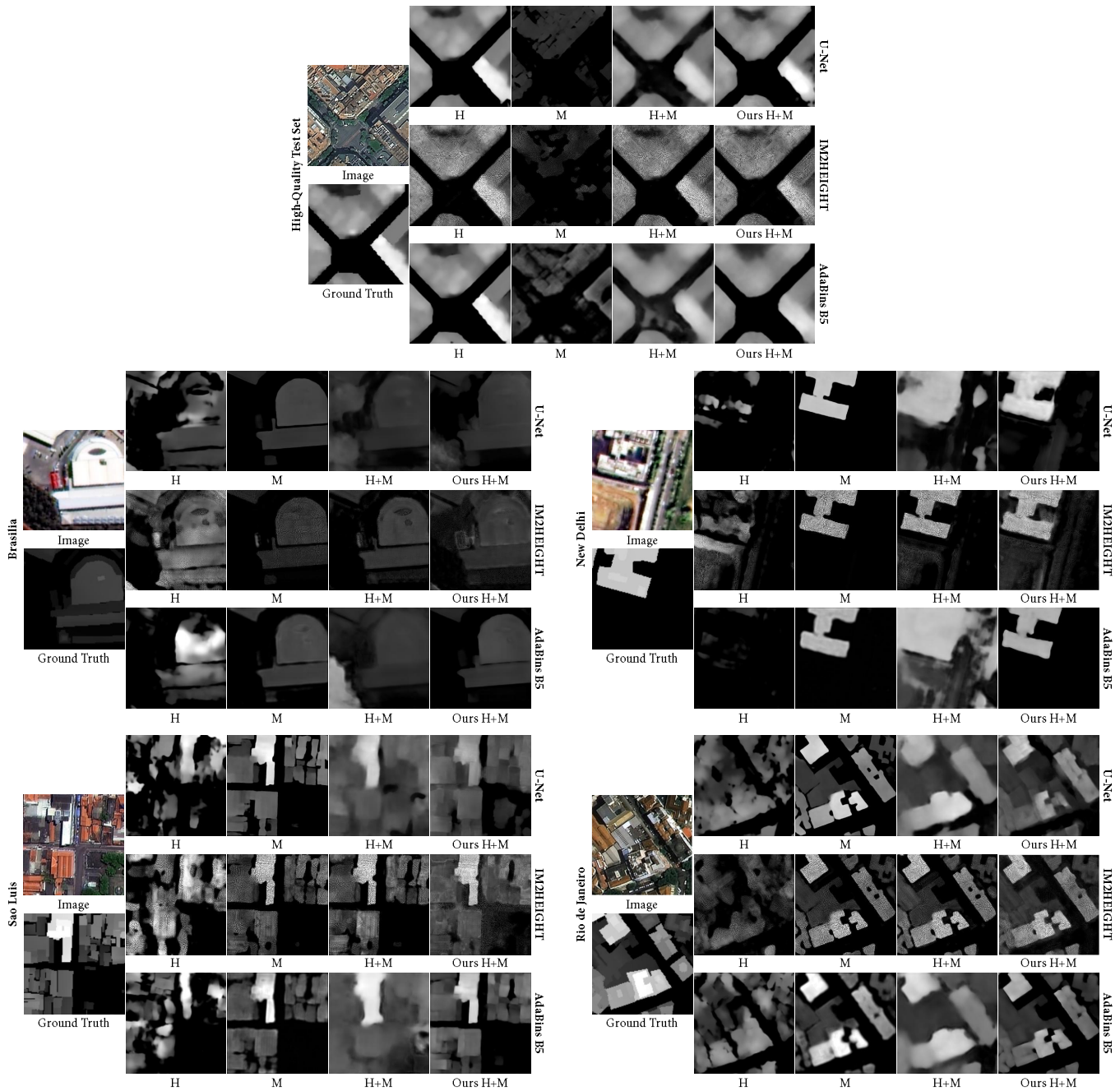


Fig. 4. Qualitative Results of Different Models on DFC23. The maps are scaled to the same range. One sample from each test set is visualized per block. Each row represents a different backbone network. H: Backbone network trained on high-quality labels only; M: Backbone network trained on mid-quality labels only; H+M: Backbone network trained on both high-quality and mid-quality labels; Ours H+M: Our proposed pipeline using the backbone network trained on both high- and mid-quality labels.

### B. Ablation Studies

In this section, we present extensive ablation studies to demonstrate the efficacy of the design modules. The experiments are conducted on both the DFC23 and GBH datasets, using our proposed pipeline, with U-Net as the backbone network.

1) *“Domain” Classifier*: The “domain” classifier is designed to distinguish underlying domains that may be implicitly encoded in the label quality distribution. It is jointly

trained with the height predictors, allowing it to introduce domain-specific information during training. In addition, it guides the aggregation of outputs from each branch during inference by assigning higher weights to the outputs from branches aligned with the inferred domain label. As shown in Table III and Table IV, the “domain” classifier can largely improve the model’s performance, especially on the out-of-domain test sets. Specifically, the average building-wise RMSE on the DFC23 dataset decreases from 8.6909 m to 4.7562 m,

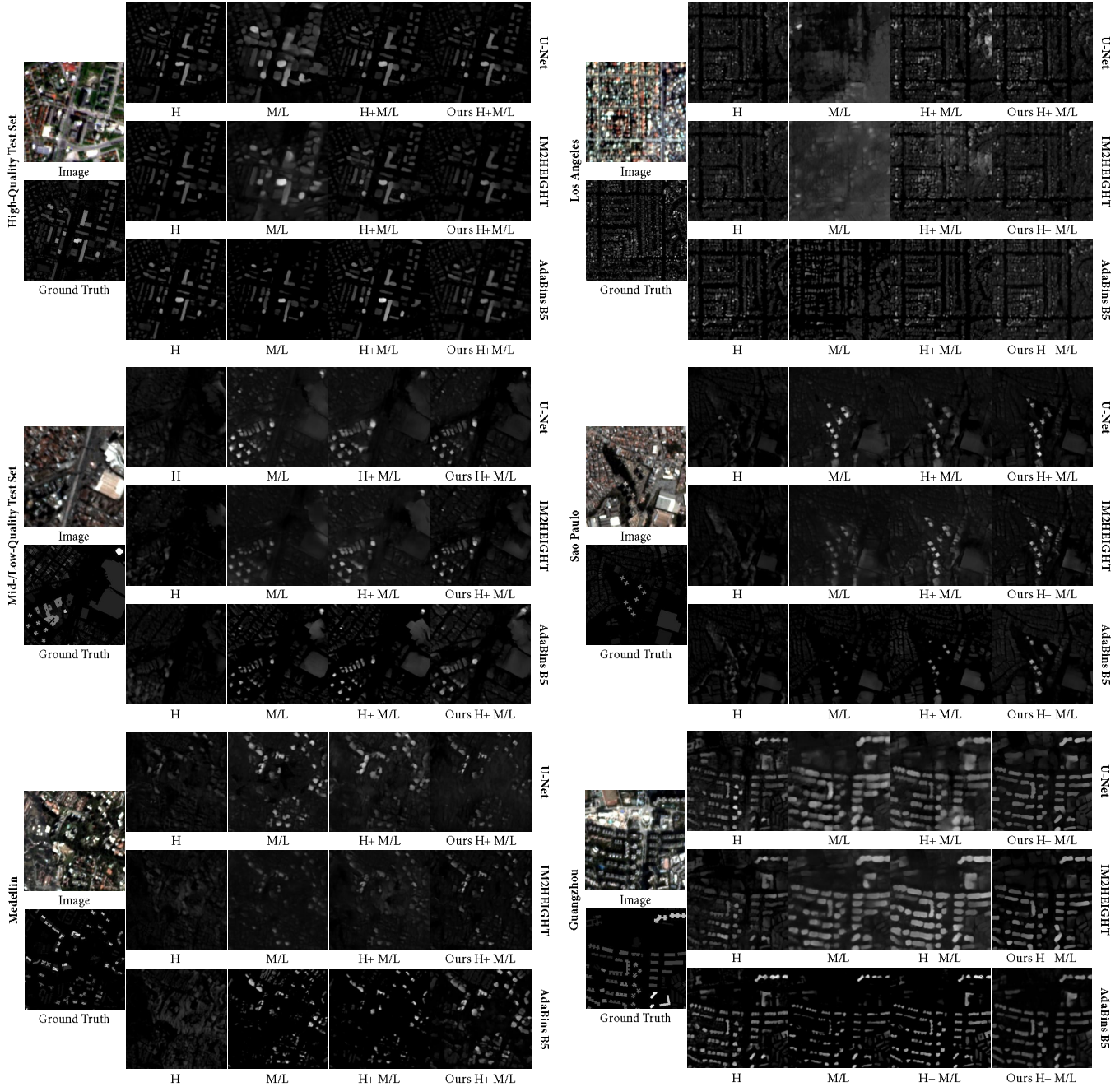


Fig. 5. Qualitative Results of Different Models on GBH. The maps are scaled to the same range. One sample from each test set is visualized per block. Each row represents a different backbone network. H: Backbone network trained on high-quality labels only; M/L: Backbone network trained on mid- and low-quality labels only; H+M/L: Backbone network trained on high-, mid- and low-quality labels; Ours H+M/L: Our proposed pipeline using the backbone network trained on high-, mid-, and low-quality labels.

representing a 45.27 % improvement. On the GBH dataset, the average building-wise RMSE improves from 7.5291 m to 7.2541 m, corresponding to a 3.65 % improvement. While the overall gain on GBH is modest, substantial improvements are observed on out-of-domain subsets, further demonstrating the effectiveness of the “domain” classifier.

2) *Balanced Soft Height Loss*: The balanced soft height loss is designed to leverage imperfect labels by filtering the supervisory signal according to absolute height values. This

approach addresses two key challenges: the presence of noise in imperfect labels, which can degrade model performance, and the imbalanced distribution of pixel-wise height values. As shown in Table III and IV, though the balanced soft height loss alone does not enhance overall performance, it can effectively mitigate the negative impact of noisy labels, resulting in more robust performance, particularly in Los Angeles. Together with other designed modules, the overall performance boost is significant. This validates the necessity of designing losses

TABLE III

ABLATION STUDIES ON DFC23. BUILDING-WISE RMSES ARE REPORTED IN METERS. THE PIPELINE IS BACKBONED BY U-NET. ENS.: ENSEMBLE;  $L_{DC}$ : DOMAIN CLASSIFIER;  $L_{BSH}$ : BALANCED SOFT HEIGHT LOSS;  $L_{OC}$ : ORDINAL CONSTRAINTS; GT AUG.: GROUND TRUTH AUGMENTATION. THE BEST IS HIGHLIGHTED IN GREEN.

Ens.	$L_{DC}$	$L_{BSH}$	$L_{OC}$	GT Aug.	In-Domain		Out-of-Domain				Average	
					High-Quality Test Set	Test Set	Brasilia	New Delhi	Sao Luis	Rio de Janeiro		Average
✓					7.4842		9.3961	8.7850	6.2896	11.4998	8.9926	8.6909
✓	✓				4.9835		2.3857	4.8198	<b>2.2624</b>	9.3292	4.6993	4.7562
✓	✓	✓			5.0231		3.1498	5.7679	2.6543	8.6232	5.0488	5.0437
✓	✓	✓	✓		<b>4.6485</b>		<b>2.1197</b>	4.8313	2.3912	8.8752	4.5544	4.5732
✓	✓			✓	5.1768		4.0525	<b>4.5670</b>	2.3442	<b>7.6107</b>	4.6436	4.7502
✓	✓	✓	✓	✓	4.8461		2.4613	4.7726	2.6402	7.9878	<b>4.4655</b>	<b>4.5416</b>

TABLE IV

ABLATION STUDIES ON GBH. BUILDING-WISE RMSES ARE REPORTED IN METERS. THE PIPELINE IS BACKBONED BY U-NET. ENS.: ENSEMBLE;  $L_{DC}$ : DOMAIN CLASSIFIER;  $L_{BSH}$ : BALANCED SOFT HEIGHT LOSS;  $L_{OC}$ : ORDINAL CONSTRAINTS; GT AUG.: GROUND TRUTH AUGMENTATION. THE BEST IS HIGHLIGHTED IN GREEN.

Ens.	$L_{DC}$	$L_{BSH}$	$L_{OC}$	GT Aug.	In-Domain			Out-of-Domain				Average	
					High-Quality Test Set	Los Angeles	Average	Mid-/Low-Quality Test Set	Sao Paulo	Medellin	Guangzhou		Average
✓					5.8309	5.4246	5.6277	11.4728	6.1393	4.6286	<b>11.6786</b>	8.4798	7.5291
✓	✓				3.7807	9.7912	6.7859	8.4418	5.5307	3.8394	12.1407	<b>7.4881</b>	7.2541
✓	✓	✓			4.2620	4.5810	4.4215	9.3561	<b>5.4464</b>	4.0296	12.4383	7.8176	6.6856
✓	✓	✓	✓		4.3612	3.8057	4.0835	8.7765	5.4832	4.0373	13.0587	7.8389	6.5871
✓	✓			✓	<b>3.6792</b>	7.0112	5.3452	<b>8.3891</b>	5.5962	6.2899	13.0767	8.3380	7.3404
✓	✓	✓	✓	✓	4.2323	<b>3.5862</b>	<b>3.9093</b>	9.2725	5.5070	<b>3.8394</b>	12.5761	7.7987	<b>6.5023</b>

that explicitly account for the uneven reliability of annotations across domains.

To further investigate the influence of hyperparameters in the soft height loss, we conducted additional experiments on the GBH dataset, as summarized in Table V. The results indicate that performance remains relatively stable across different parameter configurations, with the default settings appearing close to optimal. More specifically:

- For mid-quality labels, slightly increasing the sampling rate ( $\alpha_1$ ) can degrade overall performance. Tightening the boundaries (*i.e.*, decreasing  $\tau_1$ ) marginally improves results, though this brings more noise from the noisy labels. Conversely, relaxing the boundaries eliminates more noise but also removes more supervisory signals, leading to consistently worse performance in all domains.
- For low-quality labels, slight increases in the number of sampled pixels ( $\alpha_2$ ) can yield subtle improvements, but performance tends to plateau. Narrowing the buffer zone (*i.e.*, decreasing  $\tau_2$ ) generally enhances overall performance, whereas broadening it (*i.e.*, increasing  $\tau_2$ ) tends to degrade performance, especially on the out-of-domain test sets.
- Replacing the balanced sampling strategy with random sampling leads to a notable decline in performance, emphasizing the importance of the tailored sampling design that accounts for the imbalanced height value distribution.

3) *Ordinal Constraints*: The ordinal relations encourage the model to produce ordinally consistent predictions, serving as a complementary supervisory signal alongside the balanced soft loss. It extracts the ordinal relations from noisy height annotations, which are often more reliable than the absolute height

values. As shown in Table III and Table IV, incorporating ordinal constraints significantly improves overall performance and results in better in-domain performance, and improved balance overall. Together with the balanced soft losses, the pipelines achieve strong results, indicated by improvements of overall performance with more balanced in-domain and out-of-domain results.

To further explore the effect of different strategies for enforcing ordinal constraints, we conducted additional experiments summarized in Table VI. The results indicate that incorporating low-quality labels when computing ordinal constraints is beneficial for enhancing overall robustness, especially for improvements in in-domain results. This suggests that relatively low-quality labels can provide valuable relative information to guide learning.

Additionally, leveraging cross-image ordinal relations can yield further performance gains, particularly in out-of-domain cities, by enabling the model to generalize relative height relationships across different scenes.

All ordinal constraints are computed using a balanced sampling strategy, where pixel pairs are uniformly sampled across height differences. When this strategy is replaced by random sampling, in-domain performance drops substantially.

4) *Ground Truth Augmentation*: In the evaluation process, improvements in quantitative metrics do not always correspond to perceptual gains. By comparing the results in Table III and Table IV to the baseline networks, a model trained with all components: ensemble learning, the "domain" classifier, the balanced soft height loss, and the ordinal constraints, achieves substantially better metrics. However, when observing the visualizations in Fig. 6, the model produces over-smoothed

TABLE V

ABLATION STUDY OF HYPERPARAMETERS FOR THE BALANCED SOFT HEIGHT LOSS ON GBH. BUILDING-WISE RMSEs ARE REPORTED IN METERS. THE PIPELINE IS BACKBONED BY U-NET.  $\alpha$  IS THE SAMPLING RATIO, AND  $\tau$  IS THE THRESHOLD. THE SUBSCRIPTS "1" AND "2" DENOTE MID-QUALITY AND LOW-QUALITY LABELS, RESPECTIVELY. RANDOM SAMPLING MEANS THAT NO BALANCED SAMPLING IS CONDUCTED. THE BEST IS HIGHLIGHTED IN GREEN.

$\alpha_1$	$\tau_1$	$\alpha_2$	$\tau_2$	In-Domain			Out-of-Domain					Average
				High-Quality Test Set	Los Angeles	Average	Mid-/Low-Quality Test Set	Sao Paulo	Medellin	Guangzhou	Average	
0.1	0.3	0.1	0.5	4.2323	3.5862	3.9093	9.2725	5.5070	3.8394	12.5761	7.7987	6.5023
0.3	0.3	0.1	0.5	4.4870	4.2990	4.3930	8.5110	5.7529	3.6607	13.1274	7.7630	6.6397
0.5	0.3	0.1	0.5	4.3925	3.6758	4.0341	9.2499	5.5590	4.5100	13.3259	8.1612	6.7855
0.1	0.1	0.1	0.5	4.1332	3.3172	3.7252	8.8506	5.4144	3.7973	13.1086	7.7927	6.4369
0.1	0.5	0.1	0.5	6.3059	4.6073	5.4566	15.2756	6.3538	4.0265	14.5987	10.0636	8.5280
0.1	0.3	0.3	0.5	4.1340	3.0466	3.5903	9.0064	5.3923	3.9559	12.6697	7.7561	6.3675
0.1	0.3	0.5	0.5	4.2786	3.7872	4.0329	9.6824	5.4229	3.9600	13.2812	8.0866	6.7354
0.1	0.3	0.1	0.3	4.1514	3.2231	3.5938	8.9971	5.3609	3.9369	12.3631	7.6645	6.3388
0.1	0.3	0.1	0.7	4.2855	2.9020	3.6873	9.8572	5.5934	3.7270	13.6117	8.1973	6.6628
Random Sampling				4.2257	4.3518	4.2887	8.9230	5.4780	3.9432	13.7806	8.0312	6.7837

TABLE VI

ABLATION STUDY OF ORDINAL CONSTRAINTS ON GBH. BUILDING-WISE RMSEs ARE REPORTED IN METERS. THE PIPELINE IS BACKBONED BY U-NET. CONSTRAINT TYPES: (H+M)C+L: CROSS-IMAGE CONSTRAINTS FOR HIGH- AND MID-QUALITY LABELS, WITHIN-IMAGE CONSTRAINTS FOR LOW-QUALITY LABELS; H+M: WITHIN-IMAGE CONSTRAINTS FOR HIGH- AND MID-QUALITY LABELS; (H+M)C: HIGH- AND MID-QUALITY LABELS, CROSS-IMAGE CONSTRAINTS; H+M+L: WITHIN-IMAGE CONSTRAINTS FOR HIGH-, MID-, AND LOW-QUALITY LABELS. RANDOM SAMPLING: NO BALANCED SAMPLING OF PIXEL PAIRS IS CONDUCTED.

Constraints Type	In-Domain			Out-of-Domain					Average
	High-Quality Test Set	Los Angeles	Average	Mid-/Low-Quality Test Set	Sao Paulo	Medellin	Guangzhou	Average	
(H+M)C+L	4.2323	3.5862	3.9093	9.2725	<b>5.5070</b>	3.8394	12.5761	<b>7.7987</b>	<b>6.5023</b>
H+M	4.4211	4.1325	4.2768	9.3354	5.5368	4.2871	<b>12.4416</b>	7.9002	6.6924
(H+M)C	4.2416	3.6140	3.9278	9.1870	5.7148	6.0226	13.2404	8.5412	7.0034
H+M+L	<b>4.1428</b>	<b>2.9659</b>	<b>3.5543</b>	9.4912	5.6216	3.8501	13.2327	8.0489	6.5507
Random Sampling	4.4316	6.5894	5.5105	<b>8.7607</b>	5.7695	<b>3.8065</b>	12.8886	7.8063	7.0410

predictions, as seen in the last column. This is likely because the mid- and low-quality labels resemble smoothed versions of the true ground truth, leading the network to produce similarly smoothed outputs.

To address this issue, we introduce ground truth augmentation, which leverages the reliable predictions from the high-quality branch to enhance the mid- and low-quality annotations. This process generates more detailed supervision signals that more accurately reflect the distribution of the true ground truth. When trained on these enhanced ground truth maps, the model produces predictions with richer detail and sharper height boundaries. As demonstrated in Fig. 6, the outputs exhibit improved visual fidelity, with clearer structural details.

To prevent overfitting and enhance the flexibility of using the augmented ground truth maps, we introduce dropout on the augmentation path during training. This means the augmentation is probabilistically disabled during training. As illustrated in Table VII, by varying this probability, model performance can change, with a dropout probability of 0.3 yielding the best results.

## VII. CONCLUSIONS

In this work, we propose a novel pipeline for enhancing monocular height estimation networks using imperfect labels

through an ensemble architecture with dedicated branches specialized for different levels of label quality. Supervisory signals from imperfect labels serve as weak supervision through balanced soft height losses and ordinal relation constraints. Additionally, the predictions are sharpened via ground truth augmentation. Extensive experiments demonstrate that the proposed pipeline effectively utilizes mid-quality and low-quality labels, leading to improved overall performance across multiple domains.

The proposed approach is particularly advantageous in regions with limited label availability, making it well suited for large-scale studies. However, it does not address scenarios where labels are entirely absent. Future work could focus on extending the framework to incorporate unlabeled data to further enhance the model's generalization.

## ACKNOWLEDGEMENT

The authors would like to thank the IEEE GRSS Image Analysis and Data Fusion Technical Committee, Aerospace Information Research Institute, Chinese Academy of Sciences, Universität der Bundeswehr München, and GEOVIS Earth Technology Co., Ltd. for organizing the Data Fusion Contest, for releasing the 2023 IEEE GRSS Data Fusion Contest Dataset. The authors would like to also thank Y. Cao for providing easier access to building height data in China.

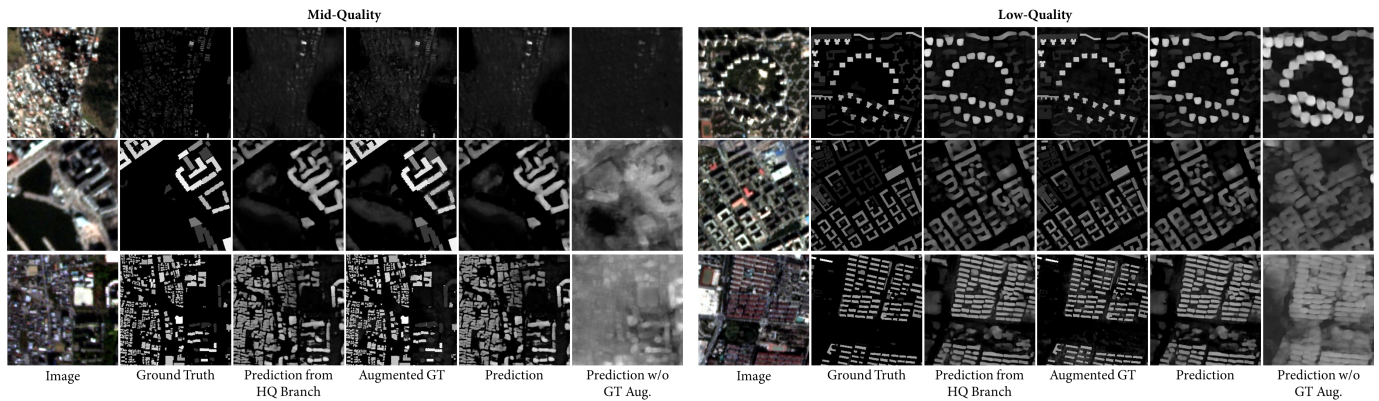


Fig. 6. Visualization of De-blurring Effect from Ground Truth Augmentation. The maps are scaled to the same range.

TABLE VII  
ABLATION STUDY OF GROUND TRUTH AUGMENTATION DROPOUT PROBABILITY ON GBH. BUILDING-WISE RMSES ARE REPORTED IN METERS. THE PIPELINE IS BACKBONED BY U-NET. THE BEST IS HIGHLIGHTED IN GREEN.

Dropout Probability	In-Domain			Out-of-Domain					
	High-Quality Test Set	Los Angeles	Average	Mid-/Low-Quality Test Set	Sao Paulo	Medellin	Guangzhou	Average	Average
0.3	4.2323	<b>3.5862</b>	<b>3.9093</b>	9.2725	5.5070	<b>3.8394</b>	<b>12.5761</b>	7.7987	<b>6.5023</b>
0.1	4.5570	6.5463	5.5517	<b>8.6084</b>	5.4523	3.8491	13.0941	<b>7.7510</b>	7.0179
0.5	4.1486	3.8777	4.0131	8.9927	5.7659	4.9133	13.4232	8.2738	6.8536
0.7	<b>3.9713</b>	3.9574	3.9644	9.9563	<b>5.4374</b>	4.1067	12.6887	8.0473	6.6863

REFERENCES

[1] S. Ural, E. Hussain, and J. Shan, “Building population mapping with aerial imagery and GIS data,” *International Journal of Applied Earth Observation and Geoinformation*, vol. 13, no. 6, pp. 841–852, Dec. 2011.

[2] M. Alahmadi, P. M. Atkinson, and D. Martin, “A Comparison of Small-Area Population Estimation Techniques Using Built-Area and Height Data, Riyadh, Saudi Arabia,” *IEEE Journal of Selected Topics in Applied Earth Observations and Remote Sensing*, vol. 9, no. 5, pp. 1959–1969, May 2016.

[3] F. Schug, D. Frantz, S. van der Linden, and P. Hostert, “Gridded population mapping for Germany based on building density, height and type from Earth Observation data using census disaggregation and bottom-up estimates,” *PLOS ONE*, vol. 16, no. 3, p. e0249044, Mar. 2021.

[4] E. Resch, R. A. Bohne, T. Kvamsdal, and J. Lohne, “Impact of Urban Density and Building Height on Energy Use in Cities,” *Energy Procedia*, vol. 96, pp. 800–814, Sep. 2016.

[5] S. Shareef, “The impact of urban morphology and building’s height diversity on energy consumption at urban scale. The case study of Dubai,” *Building and Environment*, vol. 194, p. 107675, May 2021.

[6] S. Freitas, C. Catita, P. Redweik, and M. C. Brito, “Modelling solar potential in the urban environment: State-of-the-art review,” *Renewable and Sustainable Energy Reviews*, vol. 41, pp. 915–931, Jan. 2015.

[7] L. Cheng, F. Zhang, S. Li, J. Mao, H. Xu, W. Ju, X. Liu, J. Wu, K. Min, X. Zhang, and M. Li, “Solar energy potential of urban buildings in 10 cities of China,” *Energy*, vol. 196, p. 117038, Apr. 2020.

[8] Q. Li, S. Krapf, L. Mou, Y. Shi, and X. X. Zhu, “Deep learning-based framework for city-scale rooftop solar potential estimation by considering roof superstructures,” *Applied Energy*, vol. 374, p. 123839, Nov. 2024.

[9] M. A. Bakarman and J. D. Chang, “The Influence of Height/width Ratio on Urban Heat Island in Hot-arid Climates,” *Procedia Engineering*, vol. 118, pp. 101–108, Jan. 2015.

[10] C. Xi, C. Ren, J. Wang, Z. Feng, and S.-J. Cao, “Impacts of urban-scale building height diversity on urban climates: A case study of Nanjing, China,” *Energy and Buildings*, vol. 251, p. 111350, Nov. 2021.

[11] M. Wang and H. Xu, “The impact of building height on urban thermal environment in summer: A case study of Chinese megacities,” *PLoS ONE*, vol. 16, no. 4, p. e0247786, Apr. 2021.

[12] Q. Song, C. M. Albrecht, Z. Xiong, and X. X. Zhu, “Biomass Estimation and Uncertainty Quantification From Tree Height,” *IEEE Journal of Selected Topics in Applied Earth Observations and Remote Sensing*, vol. 16, pp. 4833–4845, 2023.

[13] N. Lang, W. Jetz, K. Schindler, and J. D. Wegner, “A high-resolution canopy height model of the Earth,” *Nature Ecology & Evolution*, vol. 7, no. 11, pp. 1778–1789, Nov. 2023.

[14] J. P. Ometto, E. B. Gorgens, F. R. de Souza Pereira, L. Sato, M. L. R. de Assis, R. Cantinho, M. Longo, A. D. Jacon, and M. Keller, “A biomass map of the Brazilian Amazon from multisource remote sensing,” *Scientific Data*, vol. 10, no. 1, p. 668, Sep. 2023.

[15] M. Migliavacca, T. Musavi, M. D. Mahecha, J. A. Nelson, J. Knauer, D. D. Baldocchi, O. Perez-Priego, R. Christiansen, J. Peters, K. Anderson, M. Bahn, T. A. Black, P. D. Blanken, D. Bonal, N. Buchmann, S. Caldararu, A. Carrara, N. Carvalhais, A. Cescatti, J. Chen, J. Cleverly, E. Cremonese, A. R. Desai, T. S. El-Madany, M. M. Farella, M. Fernández-Martínez, G. Filippa, M. Forkel, M. Galvagno, U. Gomasasca, C. M. Gough, M. Göckede, A. Ibrom, H. Ikawa, I. A. Janssens, M. Jung, J. Kattge, T. F. Keenan, A. Knohl, H. Kobayashi, G. Kraemer, B. E. Law, M. J. Liddell, X. Ma, I. Mammarella, D. Martini, C. Macfarlane, G. Matteucci, L. Montagnani, D. E. Pabon-Moreno, C. Panigada, D. Papale, E. Pendall, J. Penuelas, R. P. Phillips, P. B. Reich, M. Rossini, E. Rotenberg, R. L. Scott, C. Stahl, U. Weber, G. Wohlfahrt, S. Wolf, I. J. Wright, D. Yakir, S. Zaehle, and M. Reichstein, “The three major axes of terrestrial ecosystem function,” *Nature*, vol. 598, no. 7881, pp. 468–472, Oct. 2021.

[16] O. Ronneberger, P. Fischer, and T. Brox, “U-Net: Convolutional Networks for Biomedical Image Segmentation,” *arXiv:1505.04597 [cs]*, May 2015.

[17] V. Badrinarayanan, A. Kendall, and R. Cipolla, “SegNet: A Deep Convolutional Encoder-Decoder Architecture for Image Segmentation,” *IEEE Transactions on Pattern Analysis and Machine Intelligence*, vol. 39, no. 12, pp. 2481–2495, Dec. 2017.

[18] B. Baheti, S. Innani, S. Gajre, and S. Talbar, “Eff-UNet: A Novel Architecture for Semantic Segmentation in Unstructured Environment,” in *2020 IEEE/CVF Conference on Computer Vision and Pattern Recognition Workshops (CVPRW)*. Seattle, WA, USA: IEEE, Jun. 2020, pp. 1473–1481.

[19] L. Mou and X. X. Zhu, “IM2HEIGHT: Height Estimation from Single Monocular Imagery via Fully Residual Convolutional-Deconvolutional

- Network,” *arXiv:1802.10249 [cs]*, Feb. 2018.
- [20] H. A. Amirkolae and H. Arefi, “Convolutional neural network architecture for digital surface model estimation from single remote sensing image,” *Journal of Applied Remote Sensing*, vol. 13, no. 01, p. 1, Mar. 2019.
- [21] S. Xing, Q. Dong, and Z. Hu, “Gated Feature Aggregation for Height Estimation From Single Aerial Images,” *IEEE Geoscience and Remote Sensing Letters*, pp. 1–5, 2021.
- [22] S. Chen, Y. Shi, Z. Xiong, and X. X. Zhu, “HTC-DC Net: Monocular Height Estimation From Single Remote Sensing Images,” *IEEE Transactions on Geoscience and Remote Sensing*, vol. 61, pp. 1–18, 2023.
- [23] S. Srivastava, M. Volpi, and D. Tuia, “Joint height estimation and semantic labeling of monocular aerial images with CNNs,” in *2017 IEEE International Geoscience and Remote Sensing Symposium (IGARSS)*, Jul. 2017, pp. 5173–5176.
- [24] M. E. Paoletti, J. M. Haut, P. Ghamisi, N. Yokoya, J. Plaza, and A. Plaza, “U-IMG2DSM: Unpaired Simulation of Digital Surface Models With Generative Adversarial Networks,” *IEEE Geoscience and Remote Sensing Letters*, vol. 18, no. 7, pp. 1288–1292, Jul. 2021.
- [25] Z.-H. Zhou, “A brief introduction to weakly supervised learning,” *National Science Review*, vol. 5, no. 1, pp. 44–53, Jan. 2018.
- [26] W. Chen, Z. Fu, D. Yang, and J. Deng, “Single-Image Depth Perception in the Wild,” *arXiv:1604.03901 [cs]*, Jan. 2017.
- [27] J. Lienen, E. Hullermeier, R. Ewerth, and N. Nommensen, “Monocular Depth Estimation via Listwise Ranking Using the Plackett-Luce Model,” in *Proceedings of the IEEE/CVF Conference on Computer Vision and Pattern Recognition*, 2021, pp. 14 595–14 604.
- [28] Z. Xiong and X. X. Zhu, “Knowledge Transfer for Label-Efficient Monocular Height Estimation,” in *IGARSS 2022 - 2022 IEEE International Geoscience and Remote Sensing Symposium*, Jul. 2022, pp. 5377–5380.
- [29] S. Chen, Y. Shi, and X. X. Zhu, “Long-tailed Regression with Ensembles for Monocular Height Estimation from Single Remote Sensing Images,” in *2023 Joint Urban Remote Sensing Event (JURSE)*, May 2023, pp. 1–4.
- [30] M. Izadi and P. Saeedi, “Three-Dimensional Polygonal Building Model Estimation From Single Satellite Images,” *IEEE TRANSACTIONS ON GEOSCIENCE AND REMOTE SENSING*, vol. 50, no. 6, p. 19, 2012.
- [31] S. F. Bhat, I. Alhashim, and P. Wonka, “AdaBins: Depth Estimation using Adaptive Bins,” in *2021 IEEE/CVF Conference on Computer Vision and Pattern Recognition (CVPR)*, Jun. 2021, pp. 4008–4017.
- [32] K. Sohn, D. Berthelot, N. Carlini, Z. Zhang, H. Zhang, C. A. Raffel, E. D. Cubuk, A. Kurakin, and C.-L. Li, “FixMatch: Simplifying Semi-Supervised Learning with Consistency and Confidence,” in *Advances in Neural Information Processing Systems*, vol. 33. Curran Associates, Inc., 2020, pp. 596–608.
- [33] L. Yang, L. Qi, L. Feng, W. Zhang, and Y. Shi, “Revisiting Weak-to-Strong Consistency in Semi-Supervised Semantic Segmentation,” in *Proceedings of the IEEE/CVF Conference on Computer Vision and Pattern Recognition*, 2023, pp. 7236–7246.
- [34] J.-X. Wang, S.-B. Chen, C. H. Q. Ding, J. Tang, and B. Luo, “Semi-Supervised Semantic Segmentation of Remote Sensing Images With Iterative Contrastive Network,” *IEEE Geoscience and Remote Sensing Letters*, vol. 19, pp. 1–5, 2022.
- [35] W. Huang, Y. Shi, Z. Xiong, and X. X. Zhu, “AdaptMatch: Adaptive matching for semisupervised binary segmentation of remote sensing images,” *IEEE Transactions on Geoscience and Remote Sensing*, vol. 61, pp. 1–16, 2023.
- [36] K. Heidler, I. Nitze, G. Grosse, and X. X. Zhu, “PixelDINO: Semi-Supervised Semantic Segmentation for Detecting Permafrost Disturbances in the Arctic,” *IEEE Transactions on Geoscience and Remote Sensing*, vol. 62, pp. 1–12, 2024.
- [37] Z.-H. Zhou, “Multi-Instance Learning from Supervised View,” *Journal of Computer Science and Technology*, vol. 21, no. 5, pp. 800–809, Sep. 2006.
- [38] Z.-H. Zhou and M.-L. Zhang, “Solving multi-instance problems with classifier ensemble based on constructive clustering,” *Knowledge and Information Systems*, vol. 11, no. 2, pp. 155–170, Feb. 2007.
- [39] F. Muhlenbach, S. Lallich, and D. A. Zighed, “Identifying and Handling Mislabelled Instances,” *Journal of Intelligent Information Systems*, vol. 22, no. 1, pp. 89–109, Jan. 2004.
- [40] C. Liu, C. M. Albrecht, Y. Wang, Q. Li, and X. X. Zhu, “AIO2: Online Correction of Object Labels for Deep Learning With Incomplete Annotation in Remote Sensing Image Segmentation,” *IEEE Transactions on Geoscience and Remote Sensing*, vol. 62, pp. 1–17, 2024.
- [41] Bayerische Vermessungsverwaltung, “Bayerische vermessungsverwaltung – geodaten bayern,” <http://www.geodaten.bayern.de>, accessed: 2025-05-13.
- [42] F. Biljecki, H. Ledoux, and J. Stoter, “Generating 3D city models without elevation data,” *Computers, Environment and Urban Systems*, vol. 64, pp. 1–18, Jul. 2017.
- [43] OpenStreetMap contributors, “Planet dump retrieved from <https://planet.osm.org>,” <https://www.openstreetmap.org>, 2025.
- [44] C. Liu, C. M. Albrecht, Y. Wang, and X. Xiang Zhu, “Cromss: Cross-modal pretraining with noisy labels for remote sensing image segmentation,” *IEEE Transactions on Geoscience and Remote Sensing*, vol. 63, pp. 1–17, 2025.
- [45] H. Fu, M. Gong, C. Wang, K. Batmanghelich, and D. Tao, “Deep Ordinal Regression Network for Monocular Depth Estimation,” in *2018 IEEE/CVF Conference on Computer Vision and Pattern Recognition*. Salt Lake City, UT: IEEE, Jun. 2018, pp. 2002–2011.
- [46] “2023 ieee grss data fusion contest,” Online, 2023, <https://grss-ieee.org/technical-committees/image-analysis-and-data-fusion/>.
- [47] X. Huang, L. Ren, C. Liu, Y. Wang, H. Yu, M. Schmitt, R. Hansch, X. Sun, H. Huang, and H. Mayer, “Urban Building Classification (UBC) – A Dataset for Individual Building Detection and Classification from Satellite Imagery,” in *2022 IEEE/CVF Conference on Computer Vision and Pattern Recognition Workshops (CVPRW)*. New Orleans, LA, USA: IEEE, Jun. 2022, pp. 1412–1420.